An Infrared Thermography-Based CNN System for Cultural Asset Conservation and Flooring Material Identification

Tsung-Yi Chen, Shih-Lun Chen*, Member, IEEE, Yu-Chieh Chu, Xin-Yu Chen, Pei-Chen Wu, and Patricia Angela R. Abu, Member, IEEE

***Abstract*—**Thermographic imaging has gained significant use in recent years, particularly during the epidemic, including its application in architecture for damage detection on archaeological monuments through high-temperature analysis. The non-invasive nature of Thermographic imaging, along with its ability to visualize temperature levels, allows for problem identification while preserving the building's structure. The integration of artificial intelligence further enhances its potential applications. This study aims to propose an automated inspection system using a convolutional neural network (CNN) for analyzing materials in high-temperature floor blocks. A team of academicians with more than seven years of expertise in monument preservation gathered the imaging data for this investigation. They were in charge of collecting thermal imaging photos of floors at significant monuments and aiding in the identification of overheating data and floor tile types. Analyzing materials at elevated temperatures for restoration purposes offers several benefits: efficient identification of problematic materials, identification of materials suitable for specific environmental conditions through high-temperature analysis, and determining the sequence of temperature variations among different materials to aid in restoration planning. The identification accuracy rate of this study is as high as 92.1%. Compared with the speed of 3600s for professionals to identify 100, this research only needs 3s. The efficiency is increased by about 99.91, which is an amazing improvement. These functions increase the practicality of restoration efforts, improve restoration quality and efficiency, and contribute to academic research on ancient monument preservation.

***Index Terms*—Environmental protection, monument protection, Thermographic image, CNN, image segmentation, image enhancement**

I. Introduction [1]

In recent years, the escalating global temperatures due to the impact of climate change have significantly increased the vulnerability of historical artifacts to natural degradation. This is particularly concerning for ancient structures, which have endured through vastly different environmental conditions than what exists today [1]. Furthermore, various factors, such as construction quality, material choices, and seismic events, coupled with the influence of natural elements, can contribute to the deterioration of building materials [2]. This deterioration can manifest as surface cracking, delamination at interfaces, and even the detachment of exterior facades, thereby affecting both the durability and aesthetics of structures and potentially posing public safety risks. Buildings constructed in different eras are often designed to suit the prevailing climate conditions of their time. When environmental conditions change, varying degrees of damage may result. Traditional destructive testing (DT) methods involve extracting samples from structural elements. However, one of the most important and challenging aspects of architectural restoration is achieving comprehensive and effective repair while preserving the originality and integrity of the building. Nondestructive testing (NDT) methods have emerged to address these challenges[4][5]. Through advanced technology and instrumentation, NDT can effectively detect and monitor the condition and defects of building structures, thus avoiding any compromise to their structural performance and extending their lifespan. One common NDT method is infrared Thermographic imaging, which is particularly useful for assessing building facades. When internal tiles within a building facade become detached, gaps are created. When exposed to sunlight, these gaps result in variations in Thermographic conductivity, affecting the surface temperature of the façade [6]. Thermographic images, presented as Thermographic maps, clearly display temperature distribution on the facade. By analyzing and comparing these images, cold and hot spots can be identified, pinpointing areas of tile deterioration [7]. In cases where various factors compromise the effectiveness of building insulation materials, leading to Thermographic hazards and increased energy consumption, infrared Thermographic imaging can be employed. Thermographic imaging technology has become a crucial tool across various fields, including architecture and archaeological investigations. In archaeological research, Thermographic imaging helps identify damage and understand the Thermographic properties of ancient artifacts [8]-[10]. Nonetheless, over time, the quantity of image data acquired through infrared Thermographic imaging has grown

Manuscript received XXX, 2023. This work was supported in part by the Bureau of Cultural Heritage, Ministry of Culture of Taiwan and the Ministry of Science and Technology, Taiwan, under Grant numbers of MOST-109-2410-H-197-002-MY3, MOST-108-2628-E-033-001-MY3, MOST-110-2823-8-033-002, MOST-110-2622-E-131-002, MOST-109-2622-E-131-001-CC3, MOST-108-2622-E-033-012-CC2.

S.-L. Chen, X.-Y. Chen, and P.-C. Wu, are with the Department of Electronic Engineering, Chung Yuan Christian University, Chung Li City 32023, Taiwan (e-mail: chrischen@cycu.edu.tw; s10926107@cycu.edu.tw; s10926111@cycu.edu.tw;).
T.-Y. Chen is with the Department of Electronic Engineering, Feng Chia University, Taichung, Taiwan 40724, Taiwan; (tsungychen@fcu.edu.tw).
Y.-C. Chu is with the Department of Interior Design, Chung Yuan Christian University, Chung Li City 32023, Taiwan; (yuchieh@cycu.edu.tw)
P. A. R. Abu is with the Department of Information Systems and Computer Science, Ateneo de Manila University, Quezon City 1108, Philippines (e-mail: pabu@ateneo.edu).

significantly. Dealing with such a large volume of data makes manually inspecting each image a time-consuming and labor-intensive task. Additionally, there are challenges related to the need for specialized technical skills in interpreting these images[11].

In recent years, deep learning has rapidly advanced as a cornerstone of artificial intelligence (AI) technology, demonstrating significant achievements through its integration with various domains. These research endeavors, powered by extensive datasets, have made substantial contributions to fields such as medical diagnosis, agriculture, engineering problem-solving, sentiment analysis, acoustics, personalized recommendation systems, and traffic management [12]-[20]. The application of artificial intelligence in the recognition of surface damage and material types in archaeological sites and historical building imagery has garnered increasing attention, signifying an inevitable trend. Utilized Convolutional Neural Networks (CNNs) and Artificial Neural Networks (ANNs) to identify images of immovable cultural heritage stones, discerning various stones' weathering issues. They further suggested the use of Mask R-CNN models for automated detection of stone cracks, damages, and losses within archaeological sites [21][22]. This model was trained based on evident damage in images and tested on four outdoor and two indoor views to develop a proficient recognition model[23]. Employed the Faster R-CNN model for damage detection on the rooftops of the Beijing Forbidden City, achieving average precision (AP) scores of 0.999 and 0.900. They also established an intelligent routine inspection system, simplifying the development of real-time mobile detection technology[24][25]. The Faster R-CNN model was also used for rapid automated detection of weathering and peeling damage in Beijing Forbidden City blue brick images, applicable to real-time detection systems on smartphones [26]. Through adjustments to specific link layers, modifying the number of recognition classes, and providing extensive training and validation datasets, the project achieved optimal performance while reducing training time and required computational resources. The reported results in the literature further validate the effectiveness of transfer learning, with identification accuracy reaching up to 99% [27][28], demonstrating versatility in creating different models with varying training sets and parameter configurations.

However, material identification and high-temperature recognition pose significant challenges for the technology. Therefore, this study proposes an intelligent identification system for historical site Thermographic image data and anomaly detection. The aim is to combine CNNs with Thermographic image non-destructive testing technology to develop an automated system capable of accurately identifying high-temperature anomalies, contrasting materials, and conducting heat dissipation analysis. By analyzing five CNN models (AlexNet, GoogleNet, VGG-19, SqueezeNet, and Xception), this research aims to determine the optimal recognition performance [22][23]. These findings will aid in planning restoration methods, analyzing suitable materials, and ultimately enhancing the quality and efficiency of restoration work. The novelty of this approach lies in the following aspects:

1. Special Thermographic image pre-processing method: The FILR Tool program was used to separate the temperature adjustments in the Thermographic image map to generate, and then the program was used to find out the location of the Thermographic image and crop it for storage. This method can reduce the error rate of recognizing the symptoms of High-Temperature and recognize the complete Thermographic image.

2. More efficient high-temperature analysis methods: From the results, there are five models with accuracy above 90%, and the model with the highest accuracy is AlexNet which reaches 99%. Compared with the manual identification method, the speed is 3597 seconds faster and the accuracy is improved by about 4%.

3. A novel and flexible method for monument conservation: By comparing high-temperature materials and exothermic analysis, this research can efficiently plan monument restoration, identify areas with abnormal heat dissipation, and choose appropriate conditions for restoration. This study's versatility extends to monument restoration, including common asphalt and concrete materials. The restoration techniques employed can also be adapted for other materials used in road construction. With at least three of the models achieving accuracy rates exceeding 90%, this development in flexibility can also enhance infrastructure projects.

The structure of this study is as follows: The second part is the introduction of the experimental methodology of this study. This part can be divided into 6 steps, i.e., from image preprocessing to image cutting, high-temperature symptoms, flooring, material database creation, CNN improvement, and training process, cutting image labeling and framing, and material percentage calculation. The third part shows the overall experimental results and explains the evaluation method of the model. Finally, the fourth part gives the conclusion and future outlook

II. METHODS

This study endeavors to harness the power of artificial intelligence to swiftly identify high-temperature zones in Thermographic images of historic sites. This technological capability accelerates the evaluation of site conditions by experts, streamlining the process of pinpointing areas requiring immediate restoration. Additionally, this innovative approach functions proactively by detecting excessively smooth regions that could potentially pose safety risks. The research project is structured around three fundamental elements: image processing, image segmentation, and the utilization of Convolutional Neural Networks (CNN) for recognition. It is further enriched by the incorporation of two analytical methodologies: the high-temperature material comparison technique and the exothermic analysis approach. Furthermore, this research places its primary focus on the Tainan Confucius Temple, situated in Tainan City, Southern Taiwan.

This temple, established in 1665, boasts the distinction of being Taiwan's inaugural and oldest Confucius temple. Figure. 1(a) provides a visual representation of the actual scene at the Tainan Confucius Temple. During its inception, it held a unique role as the sole institution in Taiwan dedicated to the education of children, earning it the prestigious title of the "Premier Academy of Taiwan." The Tainan Confucius Temple has maintained its significance across different political eras due to its distinctive historical and cultural value. It stands as one of Taiwan's rare and exceptionally preserved architectural treasures, carrying profound historical importance, and is

presently the foremost cultural heritage site under the safeguard of the Taiwanese government.

(a)

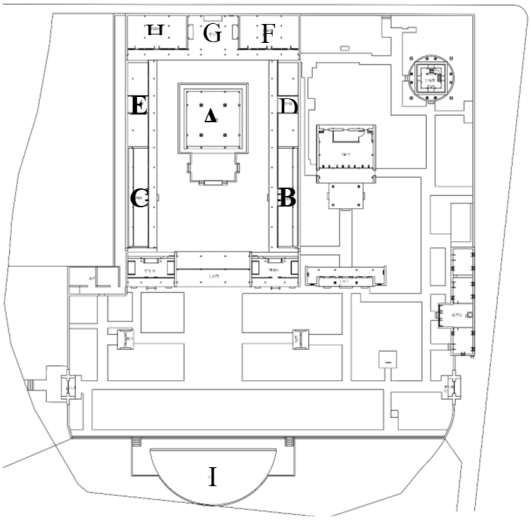

(b)

Fig.1. Da cheng Hall and surrounding spaces of the Tainan Confucius Temple. (a) Da cheng Hall. (b) Plane configuration. The core areas encompass Da Cheng Hall (code A), East Wing (code B), West Wing (code C), Ritual Implements Storeroom (code D), Musical Instrument Storeroom (code E), Yi Cheng school (code F), Chong Sheng Shrine (code G), the library housing book collections (code H), and Pan pond (code I).

The flooring materials used in areas A-H comprise approximately six different materials. This research specifically examined the four most prevalent materials, namely standard brick, asphalt, red brick, and concrete. In this research, two analytical methodologies are employed, namely the high-temperature material comparison technology and the exothermic analysis method. And the first one is the Material High-Temperature Comparative Analysis method primarily conducts high-temperature analyses on various materials to identify materials with relatively High-Temperatures. This information suggests that users should consider replacing materials with those maintaining a relatively stable (lower) temperature or prioritize repairing materials exhibiting severe high-temperature symptoms. The initial step involves identifying whether the material is part of the flooring, thereby excluding non-floor objects and simplifying subsequent material and high-temperature assessments. The subsequent steps involve determining symptoms emanating from high-temperature areas and identifying the material within these areas for further calculations. Ultimately, the percentage of high-temperature areas is computed and overlaid onto the original image to indicate materials with higher temperatures, as illustrated in Figure 1's yellow line flowchart. This serves as a reminder to users that these materials exhibit abnormal exothermic behavior [29] (prolonged High-Temperatures) and require replacement to prevent potential harm.

And the other one is the Exothermic Analysis method primarily conducts high-temperature analyses of the flooring at different times to pinpoint areas that have sustained prolonged High-Temperatures. This information alerts users to areas with a history of prolonged High-Temperatures, increasing the risk of burns. Special caution is advised when traversing such areas, and maintenance is recommended to reduce temperatures. Initially, the original image is processed to identify flooring while excluding non-floor objects. Additionally, Thermographic images from different timeframes are analyzed to determine areas with sustained High-Temperatures, with the maximum floor temperature identified. Finally, areas consistently exhibiting High-Temperatures across multiple Thermographic images are identified and labeled on the original image, denoting prolonged high-temperature exposure, as depicted in Figure 2's blue line.

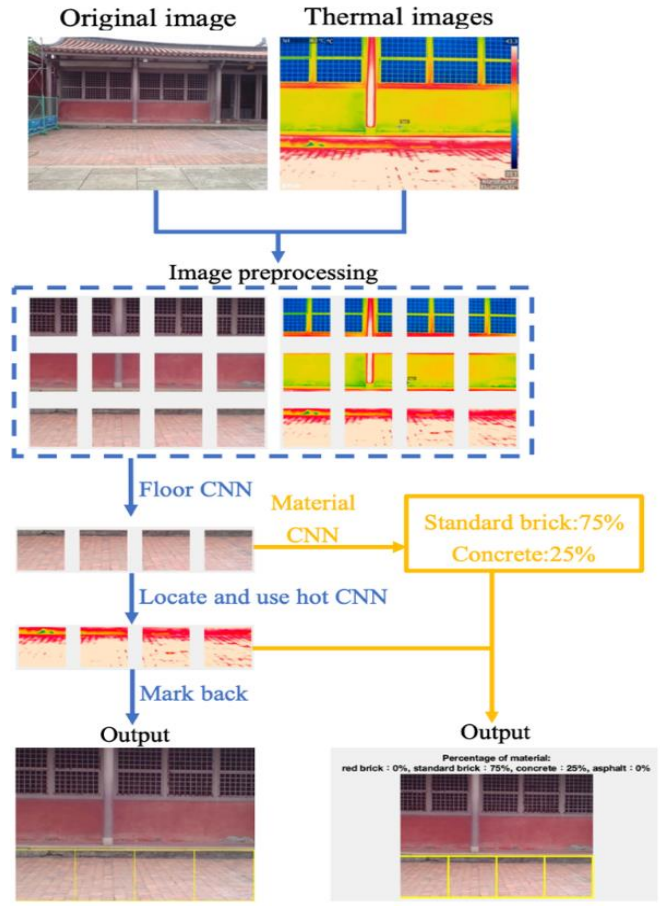

Fig.2. Flow chart of this study

The flowchart employs three types of CNN models: the model for the floor, the model for High-Temperature, and the model for the material. The training of these models will be

performed by pre-processing the original image and the Thermographic image and then cutting them into 3×4 sizes to increase the training volume, and then the CNN training will be performed for each of them until the accuracy rate is greater than 88%, at which point the training will be repeated, as shown in Figure. 3.

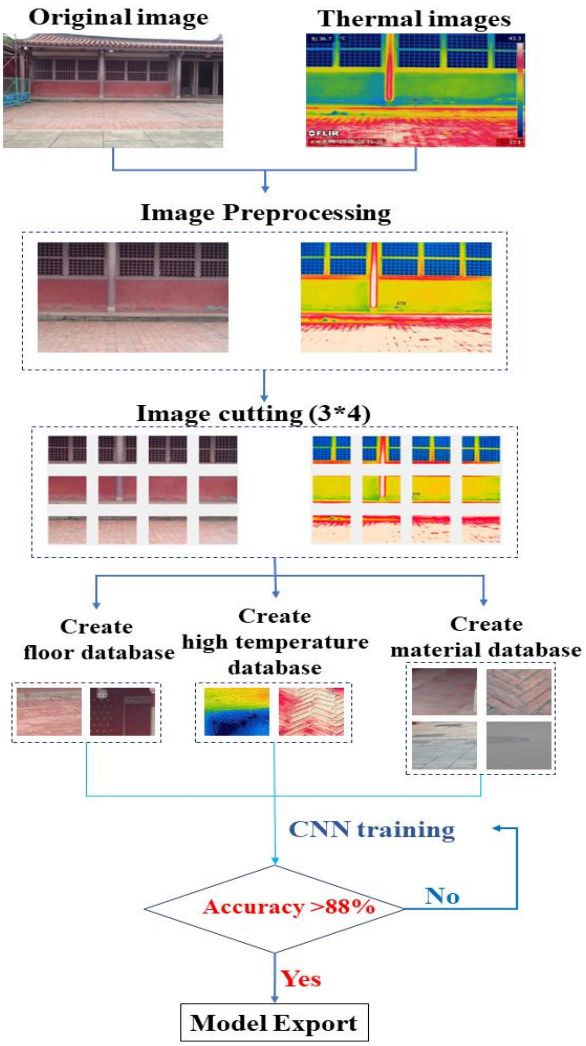

Fig.3. Model Training Flowchart

A. Image Preprocessing

1. Original drawing correction and cropping

To ensure a seamless alignment between the vulnerable regions identified in the Thermographic image and their corresponding areas in the original image, achieving identical dimensions for both images is crucial. This necessitates centering the images and removing any excess portions, as demonstrated in Figure 4. In the initial step, as shown in Figure 4 (a), the centers of the Thermographic image and the original image are aligned. This alignment establishes a common reference point for subsequent analysis and marking of the vulnerable areas. By centering the images, precise mapping and seamless integration of the Thermographic image's findings into the original image are ensured. Once the centers are aligned, both images undergo a cropping process, as depicted in Figure 4 (b). This procedure guarantees that both images share the same dimensions and eliminates any redundant areas. The resultant images can then be seamlessly merged, providing a smooth and accurate representation of the vulnerable regions within the context of the original image. By employing this cropping technique, the research aims to enhance visual consistency and precision in marking the vulnerable parts of the Thermographic image onto their corresponding locations in the original image. This approach aids in the assessment and evaluation of the site's condition, contributing to a more comprehensive understanding of the subject matter.

Fig.4. (a) Center Point Alignment. (b) Cutting results.

2. Removal of Thermographic image temperature adjustment

As color is the key determinant for identifying High-Temperatures, the temperature tones present in the Thermographic image significantly impact recognition accuracy. Therefore, it becomes imperative to eliminate these temperature tones to prevent misidentification. Initially, the temperature tones are extracted from the Thermographic image using FLIR Tools, which serves as the input tool for the Thermographic image and generates a report through its internal program, as depicted in Figure 5(a). Subsequently, the Thermographic image is cropped and resized. Given that all JPG images conform to a consistent size and fixed position once a single Thermographic image is formatted, multiple Thermographic images can be cropped and saved. This process successfully separates the Thermographic image from the temperature tones without altering the Thermographic image's display range, as demonstrated in Figure 5(b).

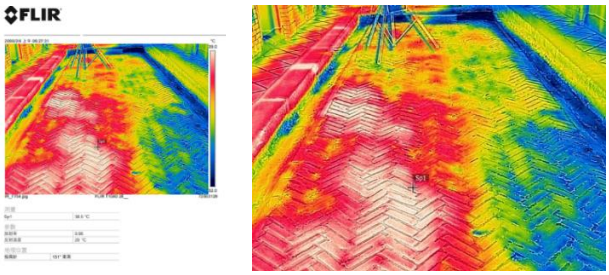

(a) (b)

Fig.5. Schematic diagram of Thermographic image acquisition. (a)Thermographic Imaging Report. (b) Image after normalized size

B. Image cutting

To address this limitation, a decision was made to divide both the original image and the Thermographic image into 12 smaller sheets, creating a grid of 3 rows and 4 columns. This approach was taken to augment the available training data and enhance the accuracy of the analysis, as illustrated in Figure 6.

By segmenting the images into smaller sheets, a more detailed and comprehensive dataset is generated for training the model. This increased amount of data allows for a more robust and accurate analysis of Thermographic patterns and facilitates the identification of vulnerable areas. Figure 6 (a) provides a visual representation of the 12 small sheets resulting from the segmentation of the original image and the Thermographic image. Each sheet represents a distinct region of interest within the overall image. Similarly, Figure 6 (b) showcases the segmented sheets in a grid-like arrangement, illustrating how the division of the images into smaller sheets enables a more granular analysis. By employing this approach, the research aims to leverage the augmented dataset obtained from the segmented sheets to improve the accuracy rate of the analysis. This enhances the ability to identify and assess vulnerable areas within the historic site based on Thermographic imaging data.

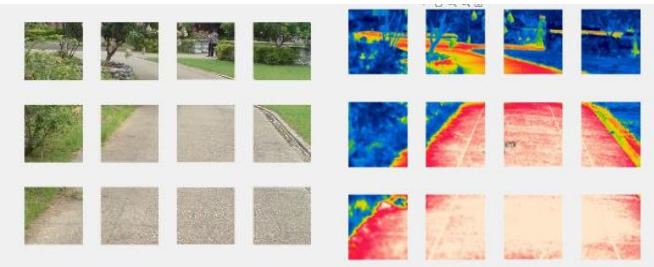

(a) (b)

Fig.6. The image is cut into 3×4 sheets. (a) Original image. (b) Thermographic image.

C. Defining model recognition objects and training sets

The artificial intelligence model training database employed in this study underwent meticulous annotation and calibration, conducted by experts and scholars boasting over seven years of experience in the field of monument maintenance. This painstakingly constructed database is designed around two distinct themes: Heritage floor tile areas and Thermographic images for High-Temperature marking, and a material-based identification database.

Firstly, there exists a CNN model training database devoted to identifying excessively high-temperature areas within historic monuments. This component is subdivided into two critical facets. The first aims to minimize error rates in subsequent high-temperature floor recognition and establish the recognition of floor locations in the original image via CNN. Adhering to the training requirements for CNN, the dataset is categorized into "floor" and "non-floor" sections, as exemplified in Figureure 7. Within the floor training dataset, a total of 1224 images, comprising both floor and non-floor scenarios, were utilized to train the foundational CNN. This dataset is further partitioned into a training set encompassing 855 images and a validation set comprising 369 images, as detailed in Table 1. The second facet encompasses the CNN dataset responsible for high-temperature recognition, illustrated in Figureure 8. Within this dataset, categories encompass red and white (indicating High-Temperatures) as well as other colors representing low temperatures and normal conditions. These distinct classifications serve as the foundation for training sets. The high-temperature recognition dataset, designated in Table II, comprises a total of 1002 images, featuring both high and low-temperature normal scenarios, catering to the second stage of CNN training. This dataset is also divided into a training set of 700 images and a validation set of 302 images, ensuring a robust training regimen.

(a) (b)

Fig.7. Schematic representation of two types of original images. (a) Floor. (b) Non-Floor.

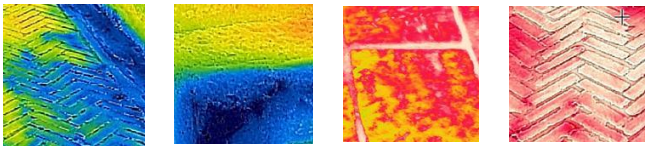

Normal Normal High-Temperature High-Temperature

Fig.8. Schematic representation of two types of Thermographic images.

Table I. Number of flooring training.

	Floor	Non-Floor
Training Data	508	347
Validation Data	219	150
Total	727	497

Table II. Number of Thermographic images training.

	High-Temperature	Normal
Training Data	350	350
Validation Data	151	151
Total	501	501

Subsequently, the CNN for material recognition was tailored to meet specific functional criteria, with a particular focus on four materials: standard bricks, asphalt, red bricks, and concrete. These materials were systematically categorized and structured into dedicated training sets, illustrated in Figure 9. Ultimately, a comprehensive dataset comprising 1685 material images was employed during the training phase of the material recognition model. This dataset underwent division into a training set, encompassing 1178 images, and a validation set, incorporating 507 images, as outlined in Table 3.

Standard Brick | Asphalt | Red Brick | Concrete

Fig.9. Schematic diagram of four target materials.

Table III. Number of image data for each material.

	Standard Brick	Asphalt	Concrete	Red Brick
Training Data	350	128	350	350
Validation Data	151	55	150	151
Total	501	183	500	501

In short, each floor, heat source and material identified by each CNN is categorized and stored and different CNNs are trained based on the amount of data in the input image.This process enables the network to learn the unique features and characteristics of floors, heat sources and materials, which can help in accurate identification of floors, heat sources and materials in subsequent analysis. In this, these specific floors, heat and materials are processed by customizing the CNNs and utilizing a well-structured training set. This research aims to improve the accuracy and reliability of material and heat identification. This approach helps advance robust material identification and analysis techniques and hyperthermia symptom analysis in the context of historic sites, providing valuable insights for preservation and restoration efforts.

D. CNN Object Recognition Training

Deep learning image classification is a fundamental component of contemporary artificial intelligence systems, enabling the recognition of intricate patterns and features within visual data. In this study, five prominent deep learning models, namely AlexNet, VGG19, GoogLeNet, SqueezeNet, and Xception, played pivotal roles as training models for identifying high-temperature symptoms, floor characteristics, and texture attributes. These models exhibit complex architectures encompassing convolutional layers, fully connected layers, and pooling layers, endowing them with remarkable proficiency in the domain of image recognition. A larger dataset facilitates the discovery of shared target characteristics during model training, enhancing effectiveness. Consequently, the dataset was expanded through the introduction of image rotations within the training set, resulting in a discernible improvement in training accuracy, as substantiated in Table IV. This approach highlights the potential of data augmentation techniques in refining deep learning image classification, thereby bolstering the accuracy and reliability of the models.

Table IV. Rotation parameters of X-axis

	Min	Max
Random rotation	-90	90
Random rescaling	1	2

The fine-tuning of training parameters plays a crucial role in optimizing the training process and enhancing the overall model accuracy. This study systematically improved training parameters to optimize the performance of the AlexNet model, ensuring its effectiveness in material recognition and analysis. The study used systematic parameter adjustment in MATLAB to improve the resilience and reliability of the training process. Eventually boosting the model's capacity to properly identify target characteristics during analysis. Additionally, this study systematically adjusted training parameters by modifying the volume base layer within the original model through transfer learning [5]. This approach not only aligned the model more accurately with the desired objectives but also increased the efficiency of the training process.

1. Two types of model training for recognizing floors and recognizing High-Temperatures.

As high-temperature recognition and floor identification fall under distinct categories, this study undertakes modifications to the original AlexNet base. The core alteration involves adjusting the fully connected_8 layers, reducing them from 1000 layers to 2 layers, and aligning the model with the research objectives. These critical modifications are detailed in Table V. Furthermore, meticulous fine-tuning of the training parameters, as elaborated in Table VI, is executed to guarantee peak model performance in alignment with the study's goals.

Table V. Network Architecture of Alexnet Model.

Layer Name	Origin	Adjust
Input	227x227x3	227x227x3
Convolution _1	55x55x96	55x55x96
Relu_1	55x55x96	55x55x96
Normalization_1	55x55x96	55x55x96
Max Pooling_1	27x27x96	27x27x96
Convolution _2	27x27x256	27x27x256
Relu_2	27x27x256	27x27x256
Normalization_2	27x27x256	27x27x256
Max Pooling_2	13x13x384	13x13x384
Convolution _3	13x13x384	13x13x384
Relu_3	13x13x384	13x13x384
Convolution _4	13x13x384	13x13x384
Relu_4	13x13x384	13x13x384
Convolution _5	13x13x256	13x13x256
Relu_5	13x13x256	13x13x256
Max Pooling_5	6x6x256	6x6x256
Fully Connected_6	1x1x4096	1x1x4096
Relu_6	1x1x4096	1x1x4096
Dropout_6	1x1x4096	1x1x4096
Fully Connected_7	1x1x4096	1x1x4096
Relu_7	1x1x4096	1x1x4096
Dropout_7	1x1x4096	1x1x4096
Fully Connected_8	1x1x1000	1x1x2
Soft Max	1x1x1000	1x1x2
Classification	1000	2

Table VI.Hyperparameter settings for high-temperature image identification network model.

	AlexNet	Google Net	Vgg19	Squeezenet	Xception
Max Epoch	100	100	100	100	100
Mini Bath Size	64	64	5	64	64
Validation Frequency	50	50	50	50	50
Validation Patience	10	10	10	10	10
Learning Rate	0.00006	0.00006	0.00006	0.00006	0.00006

2. Model training for material identification

The objective of the material recognition model is the precise identification of four distinct categories. In the course of this study, a tailored adjustment was applied to the original AlexNet architecture, specifically targeting the Fully Connected_8 layer. The pivotal alteration involved reconfiguring the initial value of 1000 to 4, thereby customizing the model to impeccably align with the research objectives, as meticulously detailed in Table VII. Furthermore, to optimize the model's performance and ensure its seamless integration with the research requirements, exhaustive fine-tuning of the training parameters was carried out. These parameters, thoughtfully elucidated in Table VIII, were subject to meticulous adjustments and calibration. The aim was to refine the model's learning process, enabling it to discern material categories with exceptional precision and efficiency.

Table VII. Network Architecture of Alexnet Model.

Layer Name	Origin	Adjust
Input	227x227x3	227x227x3
Convolution _1	55x55x96	55x55x96
Relu_1	55x55x96	55x55x96
Normalization_1	55x55x96	55x55x96
Max Pooling_1	27x27x96	27x27x96
Convolution _2	27x27x256	27x27x256
Relu_2	27x27x256	27x27x256
Normalization_2	27x27x256	27x27x256
Max Pooling_2	13x13x384	13x13x384
Convolution _3	13x13x384	13x13x384
Relu_3	13x13x384	13x13x384
Convolution _4	13x13x384	13x13x384
Relu_4	13x13x384	13x13x384
Convolution _5	13x13x256	13x13x256
Relu_5	13x13x256	13x13x256
Max Pooling_5	6x6x256	6x6x256
Fully Connected_6	1x1x4096	1x1x4096
Relu_6	1x1x4096	1x1x4096
Dropout_6	1x1x4096	1x1x4096
Fully Connected_7	1x1x4096	1x1x4096
Relu_7	1x1x4096	1x1x4096
Dropout_7	1x1x4096	1x1x4096
Fully Connected_8	1x1x1000	1x1x4
Soft Max	1x1x1000	1x1x4
Classification	1000	4

Table VIII. Hyperparameter settings for material identification network model.

	AlexNet	Google Net	Vgg19	Squeeze net	Xception
MaxEpoch	100	100	100	100	100
MiniBath Size	64	64	5	64	64
Validation Frequency	100	100	100	100	100
Validation patience	10	10	10	10	10
Learning rate	0.00006	0.00006	0.00006	0.00006	0.00006

E. Mark back to the original image

Following the correction process, the images are resized to dimensions of 640×480 pixels. To facilitate the retrieval of specific segments within the original image, a systematic numbering system is applied to the segmented images. Subsequently, each image is uniformly divided into smaller segments, each measuring 160×160 pixels. The procedure is systematically executed, commencing at the coordinates x=0 and y=0, representing the top left corner of the image. Progressing horizontally from left to right (x-direction) and vertically from top to bottom (y-direction), the image is divided into four equal parts in the x-direction (x=160, x=320, x=480) and three equal parts in the y-direction (y=160, y=320). These images are named in alphabetical order based on the number of input images. When the images are divided into a 3×4 grid, they are sequentially numbered from 1 to 12, starting from the top left corner and progressing to the bottom right corner. These segmented images are saved as Figure 10 for the original image segments and Figure 11 for the Thermographic image segments. Utilizing a designated coding methodology, the blocks identified within the Thermographic image are precisely correlated with their corresponding positions on the original map. This meticulous matching process enables the accurate localization of areas exhibiting high-temperature symptoms. These identified blocks are visually accentuated by enclosing them within bounding boxes, providing a distinct visual representation of regions displaying elevated temperature patterns. This visual highlighting aids in the differentiation and analysis of areas necessitating attention and potential restoration efforts [29]. The systematic alignment of the thermographic image with the original map, complemented by the prominent delineation of selected blocks, streamlines the process of analyzing and assessing high-temperature phenomena within the floor structure.

A1 A2 A3 A4

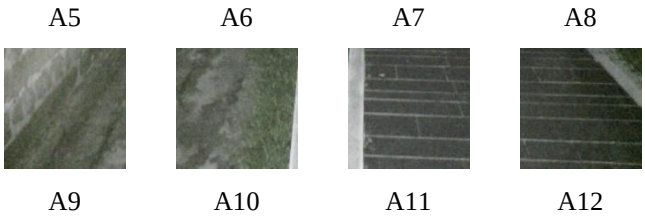

Fig.10. Schematic diagram of original image segmentation and numbering.

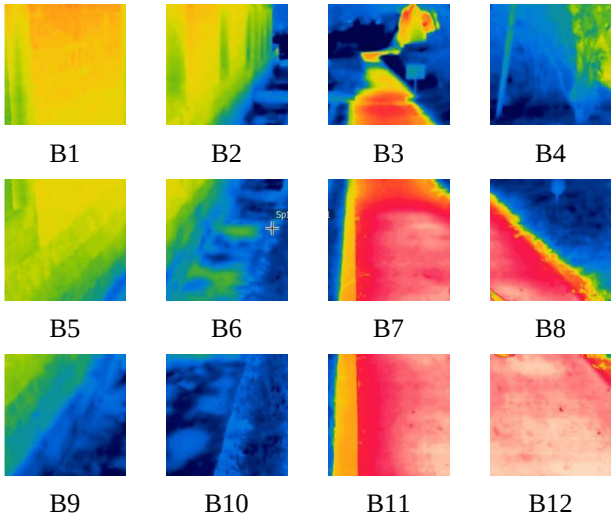

Fig.11. Schematic diagram of thermographic image segmentation and numbering.

III. Experimental Resultsnits

Within this research, the analysis of material composition entails the computation of the proportion of each material present within the high-temperature zones. This computation involves considering the total count of images identified as "High-Temperature" as the denominator in the equation. On the other hand, the numerator represents the count of sheets for each distinct material that has been detected within the High-Temperature zones in the CNN models for the material. To determine the percentage of each material, the numerator is divided by the denominator, and the result is multiplied by 100, as clearly depicted in Formula (1).

$$\frac{(Total\ number\ of\ sheets\ of\ material\ 1)}{(Total\ number\ of\ sheets\ of\ high\ temperature\ material)} \times 100\%. \quad (1)$$

This approach allows for a quantitative analysis of the distribution and prevalence of different materials within the regions exhibiting elevated temperatures. By calculating the percentage of each material, valuable insights can be derived regarding the material makeup and its relative contribution to the high-temperature areas. Such information is crucial for understanding the composition of the structure, identifying potential material-related issues, and facilitating appropriate maintenance and preservation strategies. Throughout the research endeavor, a strategic approach was employed to enhance the training dataset, aiming for improved training outcomes. This enhancement process involved various techniques such as horizontal mirroring, vertical flipping, and adjustments to rotation and scaling parameters. By implementing these techniques, the number of images within the training dataset expanded to four times the original count, as evidenced in Table IX and Table X.

Table IX. Floor and High-Temperature Training Set Increment

	Original	Adjustment	Total
Floor	1224	3672	4896
High-Temperature	1002	3006	4008

Table X.Material Training Set Increment

	Original	Adjustment	Total
Standard Brick	501	1503	2004
Asphalt	183	3006	732
Concrete	500	1500	2000
Red Brick	501	1503	2004

This study harnessed three distinct types of CNNs tailored to its specific requirements: one for floor identification, another for detecting high-temperature regions, and a third for material recognition. To comprehensively evaluate the performance of these meticulously trained models, a sophisticated analysis technique known as the confusion matrix analysis [21] was employed. The confusion matrix is a fundamental tool in assessing the performance of machine learning and artificial intelligence models. It provides a comprehensive breakdown of predictive accuracy, categorizing model outcomes into four key metrics: True Positives (correctly predicted positive samples), True Negatives (correctly predicted negative samples), False Positives (incorrectly predicted positive samples), and False Negatives (incorrectly predicted negative samples). These metrics enable a granular evaluation of a model's precision, recall, specificity, and accuracy. The confusion matrix is invaluable for understanding a model's ability to correctly classify and discriminate between different categories, making it an essential component of model evaluation and refinement in various domains, including healthcare, finance, and image recognition.

$$\text{Accuracy} = \frac{\text{TP} + \text{TN}}{\text{TP} + \text{FP} + \text{FN} + \text{TN}} \quad (2)$$

Figures 12 and 13 depict the confusion matrix outcomes for the CNN model tasked with identifying the floor within the original image and detecting areas of excessive temperature in the Thermographic image. Impressively, the accuracy rates stand at 93% and 99%, respectively.

Furthermore, Figure 14 illustrates the model's performance in discerning various floor tile materials, achieving a remarkable accuracy rate of 96%. These results are undeniably promising and constitute a significant achievement in the study. They underscore the effectiveness and reliability of the model's capabilities, signifying a crucial milestone in the research's pursuit of accurate identification and analysis within the field.

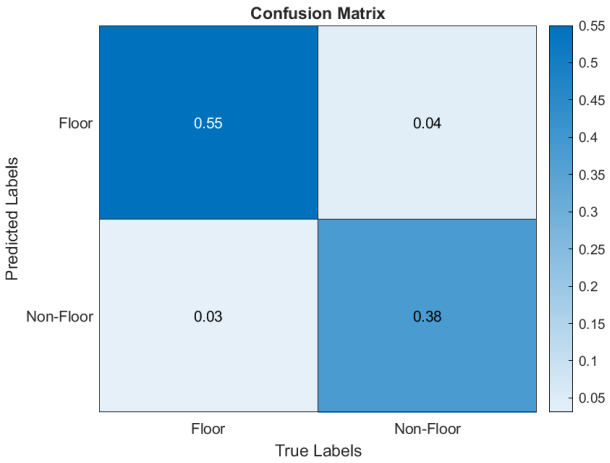

Fig.12. Confusion matrices for floor identification.

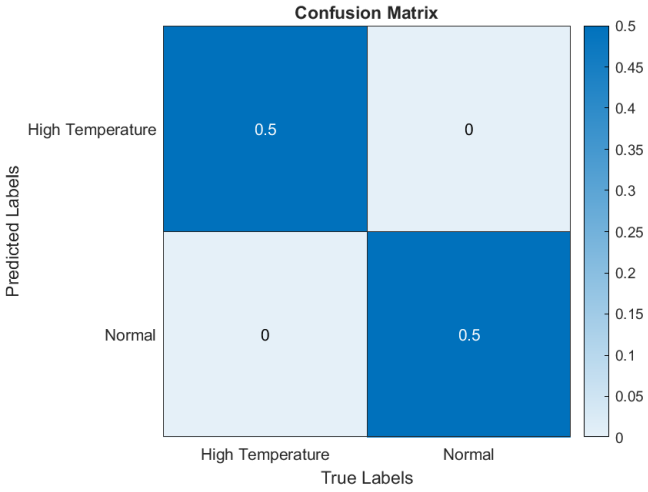

Fig.13. Confusion matrices for detecting high-temperature regions.

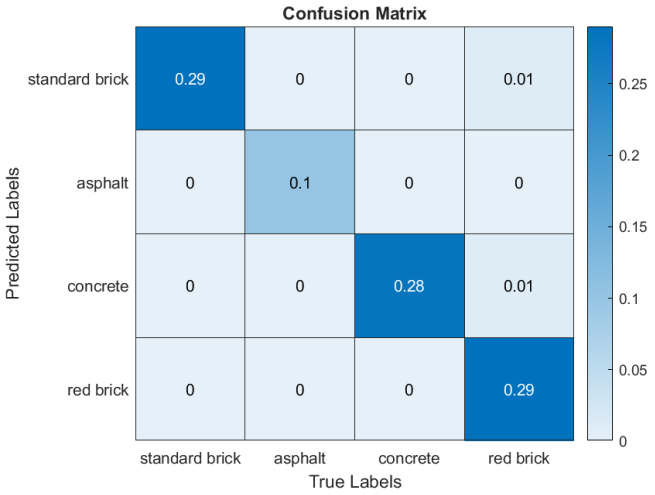

Fig.14. Confusion matrices for material recognition.

Furthermore, this study conducted an extensive analysis using five prominent CNN models, namely AlexNet, VGG19, GoogLeNet, SqueezeNet, and Xception, to determine the optimal model for the task. Employing the same dataset and parameters, the results of these three analyses are summarized in Table XI. The training processes for each model targeting the three recognition objectives are visually presented in Figures 15 to 17. The five CNN models consistently achieved a remarkable 90% accuracy in identifying high-temperature areas on the floor, with the Alexnet model notably reaching an impressive 99.7% accuracy. These outcomes reaffirm the AI model's exceptional performance in high-temperature area identification within image analysis. While these models perform commendably in identifying the floor and floor tile material within the original image, the Xception model's performance fell short of expectations, with accuracy rates below 85%. Given this significant deviation from the other models, Xception is not employed for either recognition project. These findings contribute valuable insights into selecting the most suitable model for accurate high-temperature area analysis on the floor.

Table XI.Comparison of model accuracy for flooring

	AlexNet	GoogLeNet	VGG19	SqueezeNet	Xception
floor	93.46%	94.28%	91.01%	89.37%	73.57%
high-temperature	99.7%	99%	99.33%	98.67%	96.33%
material	93.24%	92.87%	95.25%	88.91%	80.40%

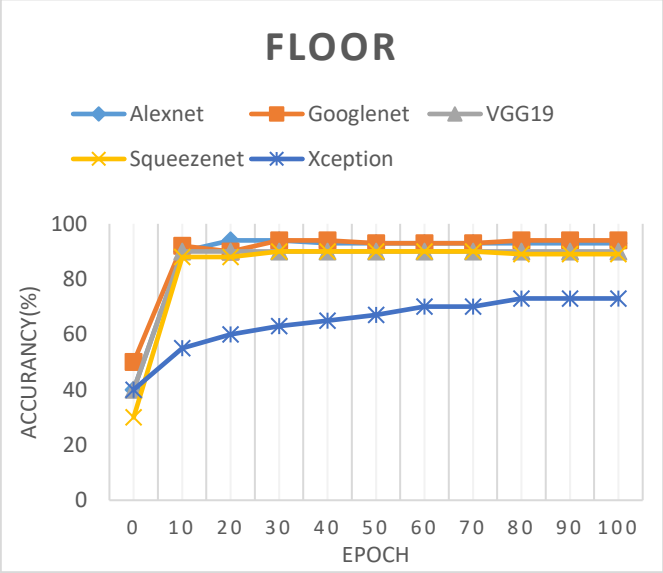

Fig.15. Model training folding chart for flooring

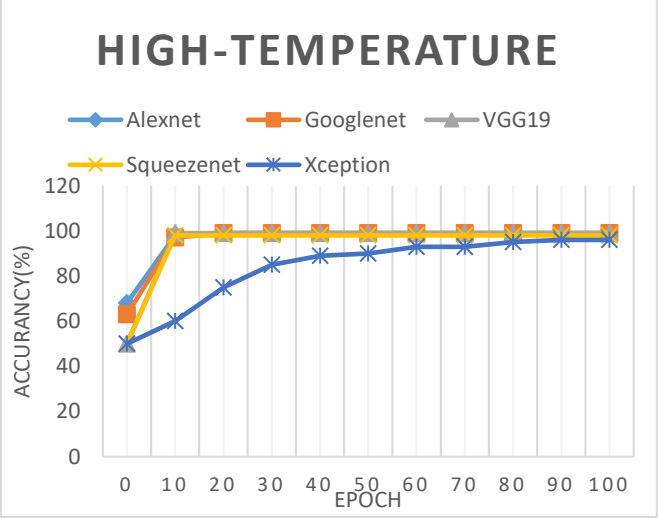

Fig.16. Model training folding chart for High-Temperatures

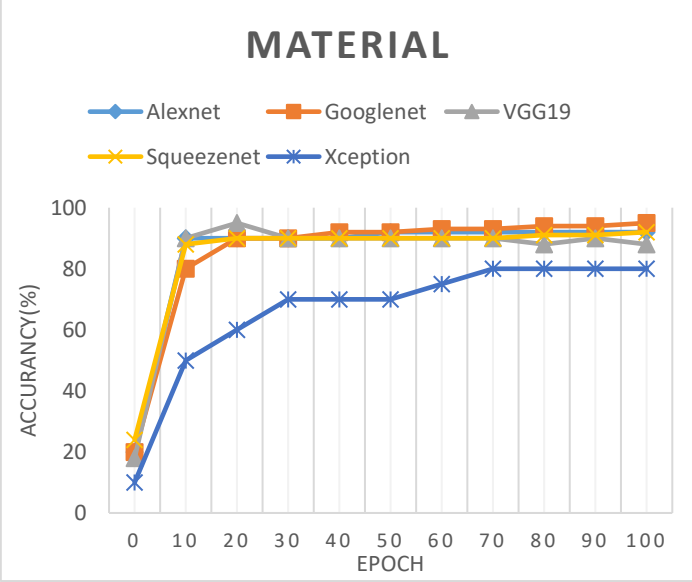

Fig.17. Model training folding chart for High-Temperatures materials.

In this research, an in-depth investigation was conducted for each recognition model, ensuring that their accuracy exceeded 88%. To further enhance recognition accuracy, the study introduced the utilization of fuzzy control techniques for additional optimization. By comparing model results, if three or more models reached a consensus on a specific identification result, that result was adopted; otherwise, no result was output. Specifically, for the recognition of floor areas, fuzzy control was introduced. This approach involved the use of four high-accuracy models, namely AlexNet, VGG19, GoogLeNet, and SqueezeNet. Through this method, an astonishing accuracy of 98.45% was achieved in the testing of 1224 samples. Compared to the original single-model recognition with the highest accuracy of GoogleNet at 94.51%, this represented an improvement of over 3%, providing strong evidence for the feasibility and accuracy enhancement achieved through fuzzy control in floor model recognition. Similarly, fuzzy control was incorporated into high-temperature recognition. It involved the analysis of five high-accuracy models: AlexNet, VGG19, GoogLeNet, SqueezeNet, and Xception, using a voting mechanism. This resulted in an impressive accuracy of 99.8% on a test set of 1002 samples. Compared to the original 99.63%, this marked a significant improvement and contribution. Finally, in the brick material recognition model, four high-accuracy models—AlexNet, VGG19, GoogLeNet, and SqueezeNet—were employed. Through the implementation of fuzzy control techniques, a high accuracy of 99.1% was achieved in the testing of 1685 samples. This reaffirmed the effectiveness and refinement of recognition assistance and correction compared to the single-model recognition result of 95.25%.

Table XII. **Results for Fuzzy**

	This work					
	GoogLe Net	Alex Net	VGG 19	Squeeze net	Xception	Result of Fuzzy
floor	93.46%	94.28%	91.01%	89.37%	N/A	98.45%
high-temperature	99%	99%	99.33%	98.67%	96.33%	99.8%
material	93.24%	92.87%	95.25%	88.91%	N/A	91.1%

The analysis generates two images as output. The first image superimposes boxes on the original image to highlight regions displaying High-Temperature symptoms, while the second image presents the corresponding thermal image. Figure 18 displays the thermal image obtained from the analysis. Moreover, the analysis furnishes information concerning the distribution of materials within the High-Temperature areas. In the upper column of the output image, the percentage of each material present in the identified High-Temperature region is presented. Notably, the results shown in Figure 18 and Figure 19 indicate that red brick exhibits the highest susceptibility in the given environment. Following red brick, standard brick

displays a lower degree of vulnerability, while concrete material demonstrates the least susceptibility to High-Temperature effects. The identification of the most vulnerable materials, such as red brick, enables the development of appropriate maintenance and preservation strategies to mitigate potential risks and ensure the longevity of historic sites. These findings underscore the significance of employing thermal imaging and material identification techniques to prioritize areas requiring attention and implement targeted interventions to safeguard vulnerable materials.

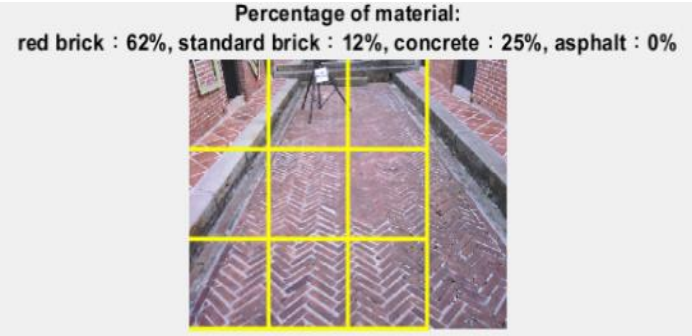

Fig.18. The actual use of the results of this study

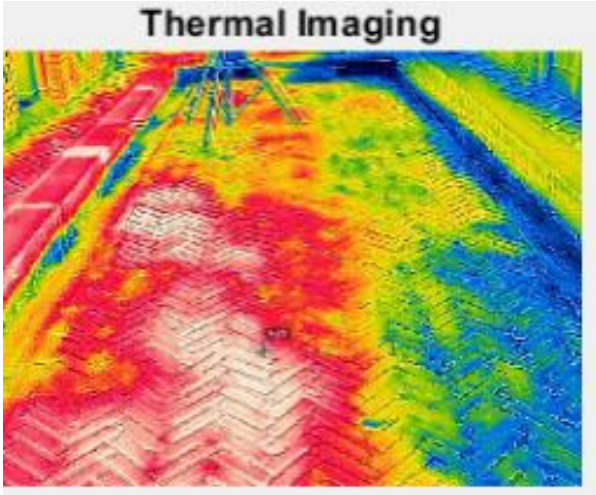

Fig.19. The actual use of the results of this study

In the original image (Figure 20), a yellow box is employed to delineate the floor area that has experienced prolonged exposure to high temperatures. Subsequently, two thermographic images, representing morning and evening conditions, are provided. In both these images, the same high-temperature area is highlighted with a yellow box for ease of reference (Figure 21 and Figure 22). This method serves a dual purpose.

Firstly, it serves as a safety warning, drawing attention to the high-temperature area and mitigating the risk of burns. Secondly, it facilitates the comparison of high-temperature materials. In cases where the ratio of high-temperature occurrences is the same, making it difficult to determine the order of priority, a comparison of the heat generation condition enables us to assess which material is more susceptible to damage and make a more informed decision. This research offers valuable insights into these applications.

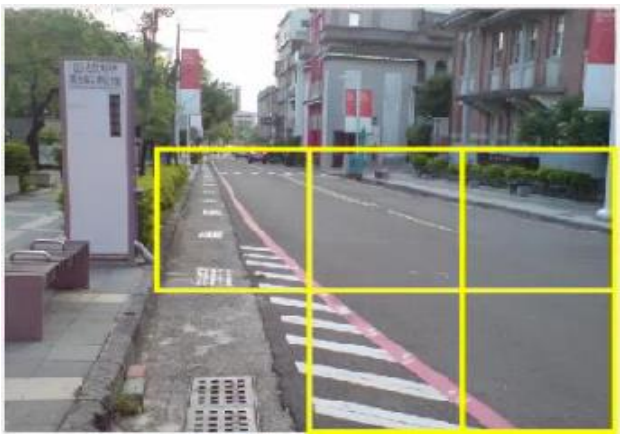

Fig.20. The actual use of the results of this study

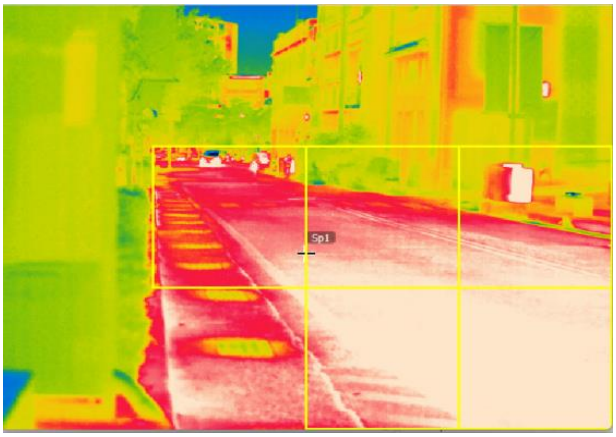

Fig.21. The actual use of the results of this study

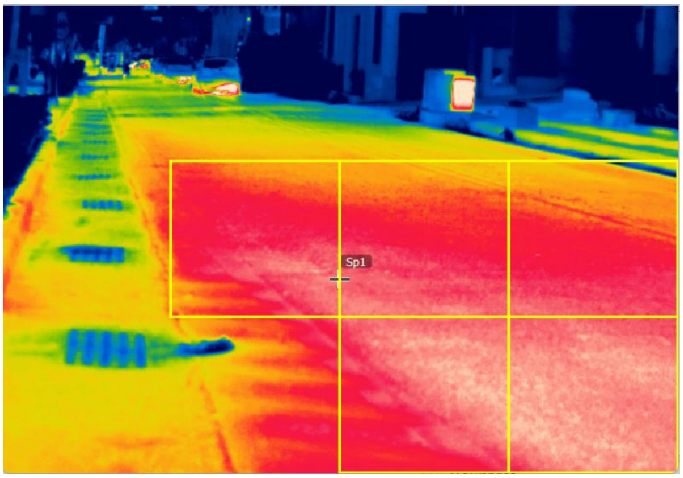

Fig.22. The actual use of the results of this study

Furthermore, this study conducted a comparison between professional manual recognition and the proposed method in terms of accuracy and time efficiency for evaluating 100 images. The results revealed that while manual recognition achieved a slightly higher accuracy rate of approximately 3%, the proposed method demonstrated a remarkable improvement in speed, requiring only 3 seconds to recognize the entire set of images. This represents an impressive enhancement of approximately

99.16%. The experimental findings indicate that the proposed approach significantly contributes to time-saving and enhances overall work efficiency, as illustrated in Table XVII.

Table XIII. Material CNN Accuracy

	Manual Judgment	Method in [30]	**This research**
Accuracy (%)	95.8%	73.5%	99.16%
Elapsed time(s)	3600	388	3

I. Conclusion

This study underscores the impact of increasing temperatures on historical sites and the necessity for proactive measures to mitigate potential harm. The comparative analysis of high-temperature materials focused on specific flooring materials, including red brick, concrete floor tiles, asphalt, and square tiles. It highlights the importance of effective material identification and analysis for selecting materials suitable for diverse environmental conditions and supporting restoration efforts. The study achieved an impressive 93% accuracy in CNN identification, which significantly contributed to the precision in detecting High-Temperature symptoms and materials. Material identification accuracy reached 93%, while the accuracy for High-Temperature areas reached 98%, marking a significant success in the precise identification and classification of materials based on their response to high temperatures. The exothermic analysis method effectively detected high-temperature zones in flooring materials and assessed whether these materials had been subjected to prolonged high-temperature conditions. This is crucial as long-term exposure to high temperatures can reduce material service life and pose burn risks on high-temperature floors, necessitating cooling maintenance. In conclusion, the accuracy rates achieved by both analysis methods validate the effectiveness of the developed approach and the reliability of the material identification system. However, research limitations include variations in training data volume and inconsistent camera angles, which can introduce errors in material assessment. Future work involves collaboration with the Cultural Affairs Bureau to obtain a larger, more consistent sample. Importantly, the study's significance extends beyond historical sites, as the methods can be applied to various material types in road construction, contributing to resilient infrastructure development. Expanding the study's scope has the potential to benefit a broader range by addressing rising temperature challenges and promoting sustainable practices in construction and maintenance. Further research and collaboration can apply these findings to preserve cultural heritage and foster sustainable infrastructure development.

References

[1] Preda, A., & Scurtu, I. C. (2019). Thermographic image building inspection for heat loss diagnosis. *Journal of Physics: Conference Series*, *1297*(1), 012004. https://doi.org/10.1088/1742-6596/1297/1/012004

[2] .Brooke, C. (2018). Thermographic Imaging for the Archaeological Investigation of Historic Buildings. Remote Sensing, 10(9), Article 9. https://doi.org/10.3390/rs10091401

[3] Siegel, J. R. H., M. Pinar Mengüc, Kyle Daun, Robert. (2020). Thermographic Radiation Heat Transfer (7th ed.). CRC Press. https://doi.org/10.1201/9780429327308

[4] Tirupathamma, M., & Niranjan, V. (2020). PRINCIPLES AND APPLICATIONS OF INFRARED THERMOGRAPHIC IMAGING. Telecommunications and Radio Engineering, 79(13). https://doi.org/10.1615/TelecomRadEng.v79.i13.70

[5] Proszak-Miąsik, D. (2019). USE OF THERMOGRAPHIC IMAGING IN CONSTRUCTION. Informatyka Automatyka Pomiary w Gospodarce i Ochronie Środowiska, 9, 12–15. https://doi.org/10.5604/01.3001.0013.2540

[6] Thomas, H. (2018). Some like it hot: The impact of next generation FLIR Systems Thermographic cameras on archaeological thermography. Archaeological Prospection, 25(1), 81–87. https://doi.org/10.1002/arp.1588

[7] J. Ahmad, A. Akula, R. Mulaveesala, and H. K. Sardana, 'Probability of Detecting the Deep Defects in Steel Sample Using Frequency Modulated Independent Component Thermography', IEEE Sensors Journal, vol. 21, no. 10, pp. 11244–11252, May 2021. https://doi.org/10.1109/JSEN.2020.3021118.

[8] Kordatos, E. Z., Exarchos, D. A., Stavrakos, C., Moropoulou, A., & Matikas, T. E. (2013). Infrared thermographic inspection of murals and characterization of degradation in historic monuments. *Construction and Building Materials*, *48*, 1261–1265. https://doi.org/10.1016/j.conbuildmat.2012.06.062

[9] ElMasry, G., ElGamal, R., Mandour, N., Gou, P., Al-Rejaie, S., Belin, E., & Rousseau, D. (2020). Emerging Thermographic imaging techniques for seed quality evaluation: Principles and applications. *Food Research International*, *131*, 109025. https://doi.org/10.1016/j.foodres.2020.109025

[10] G. Dua, V. Arora, and R. Mulaveesala, 'Defect Detection Capabilities of Pulse Compression Based Infrared Non-Destructive Testing and Evaluation', IEEE Sensors Journal, vol. 21, no. 6, pp. 7940–7947, Mar. 2021, https://doi.org/10.1109/JSEN.2020.3046320.

[11] 弘一川西, 詳悟林, 和明橋本, 勲氏家, & 邦釘全. (2020). 赤外線サーモグラフィ法における損傷自動判別技術. *Ai・データサイエンス論文集*, *1*(J1), 382–391. https://doi.org/10.11532/jsceiii.1.J1_382

[12] Chauhan, R., Ghanshala, K. K., & Joshi, R. C. (2018). Convolutional Neural Network (CNN) for Image Detection and Recognition. *2018 First International Conference on Secure Cyber Computing and Communication (ICSCCC)*, 278–282. https://doi.org/10.1109/ICSCCC.2018.8703316

[13] Almisreb, A. A., Jamil, N., & Din, N. M. (2018). Utilizing AlexNet Deep Transfer Learning for Ear Recognition. *2018 Fourth International Conference on Information Retrieval and Knowledge Management (CAMP)*, 1–5. https://doi.org/10.1109/INFRKM.2018.8464769

[14] A. Galván-Hernández, J. R. Ticay-Rivas, V. Alonso-Eugenio, V. Araña, and F. Cabrera, 'Thermographic image super-resolution based on neural networks', in *2022 3rd URSI Atlantic and Asia Pacific Radio Science Meeting (AT-AP-RASC)*, May 2022, pp. 1–4. https://doi.org/10.23919/AT-AP-RASC54737.2022.9814417.

[15] A. Ajit, K. Acharya, and A. Samanta, 'A Review of Convolutional Neural Networks', in *2020 International Conference on Emerging Trends in Information Technology and Engineering (ic-ETITE)*, Feb. 2020, pp. 1–5. doi: 10.1109/ic-ETITE47903.2020.049.

[16] M. E. Hatır, İ. İnce, and M. Korkanç, 'Intelligent detection of deterioration in cultural stone heritage', *Journal of Building Engineering*, vol. 44, p. 102690, Dec. 2021, https://doi.org/10.1016/j.jobe.2021.102690.

[17] Wang, J., & Li, Z. (2018). Research on Face Recognition Based on CNN. IOP Conference Series: Earth and Environmental Science, 170(3), 032110. https://doi.org/10.1088/1755-1315/170/3/032110

[18] Salehi, A. W., Khan, S., Gupta, G., Alabduallah, B. I., Almjally, A., Alsolai, H., Siddiqui, T., & Mellit, A. (2023). A Study of CNN and Transfer Learning in Medical Imaging: Advantages, Challenges, Future Scope. Sustainability, 15(7), Article 7. https://doi.org/10.3390/su15075930

[19] Alom, M. Z., Taha, T. M., Yakopcic, C., Westberg, S., Sidike, P., Nasrin, M. S., Van Esesn, B. C., Awwal, A. A. S., & Asari, V. K. (2018). The History Began from AlexNet: A Comprehensive Survey on Deep Learning Approaches (arXiv:1803.01164). arXiv. https://doi.org/10.48550/arXiv.1803.01164

[20] Weiss, K., Khoshgoftaar, T. M., & Wang, D. (2016). A survey of transfer learning. Journal of Big Data, 3(1), 9. https://doi.org/10.1186/s40537-016-0043-6

[21] Li, J., Deng, M., Gao, L., Yen, S., Katayama, Y., & Gu, J.-D. (2021). The

active microbes and biochemical processes contributing to deterioration of Angkor sandstone monuments under the tropical climate in Cambodia – A review. Journal of Cultural Heritage, 47, 218–226. https://doi.org/10.1016/j.culher.2020.10.010
[22] Lee, S., Moon, H., Choi, Y., & Yoon, D. K. (2018). Analyzing Thermographic Characteristics of Urban Streets Using a Thermographic Imaging Camera: A Case Study on Commercial Streets in Seoul, Korea. Sustainability, 10(2), Article 2. https://doi.org/10.3390/su10020519
[23] Özyurt, F. (2020). Efficient deep feature selection for remote sensing image recognition with fused deep learning architectures. The Journal of Supercomputing, 76(11), 8413–8431. https://doi.org/10.1007/s11227-019-03106-y
[24] Chollet, F. (2017). Xception: Deep Learning with Depthwise Separable Convolutions (arXiv:1610.02357). arXiv. https://doi.org/10.48550/arXiv.1610.02357
[25] Zeng, G. (2020). On the confusion matrix in credit scoring and its analytical properties. Communications in Statistics - Theory and Methods, 49(9), 2080–2093. https://doi.org/10.1080/03610926.2019.1568485
[26] Resende, M. M., Gambare, E. B., Silva, L. A., Cordeiro, Y. de S., Almeida, E., & Salvador, R. P. (2022). Infrared Thermographic imaging to inspect pathologies on façades of historical buildings: A case study on the Municipal Market of São Paulo, Brazil. *Case Studies in Construction Materials*, *16*, e01122. https://doi.org/10.1016/j.cscm.2022.e01122
[27] Grinzato, E., Vavilov, V., & Kauppinen, T. (1998). Quantitative infrared thermography in buildings. Energy and Buildings, 29(1), 1–9. https://doi.org/10.1016/S0378-7788(97)00039-X
[28] A definition of cultural heritage: From the tangible to the intangible. (2010). *Journal of Cultural Heritage*, *11*(3), 321–324. https://doi.org/10.1016/j.culher.2010.01.006
[29] Li, D., Liu, P., Zhang, Z., Zhang, L., Deng, J., Wang, Z., Dorrell, D. G., Li, W., & Sauer, D. U. (2022). Battery Thermographic Runaway Fault Prognosis in Electric Vehicles Based on Abnormal Heat Generation and Deep Learning Algorithms. IEEE Transactions on Power Electronics, 37(7), 8513–8525. https://doi.org/10.1109/TPEL.2022.3150026
[30] H. Du, S. He, B. Sheng, L. Ma, and R. W. H. Lau, "Saliency-Guided Color-to-Gray Conversion Using Region-Based Optimization," IEEE Transactions on Image Processing, vol. 24, no. 1, p. 434–443, 2015.

Tsung-Yi Chen received the B.S. and Ph.D. degrees from Chung Yuan Christian University, Zhongli, Taoyuan, Taiwan, in 2020, and 2023, respectively, all in electrical engineering. Since 2023, Dr. Chen has been an Assistant Professor with the Department of Electrical Engineering, Feng Chia University in Taiwan. His current research interests include VLSI chip design, image processing, internet of things, fuzzy logic control, wearable devices, machine learning, and biomedical signal processing.

Shih-Lun Chen (M'12) received the B.S. M.S., and Ph.D. degrees from National Cheng Kung University, Tainan, Taiwan, in 2002, 2004, and 2011, respectively, all in electrical engineering. He was an Assistant Professor with the Department of Electronic Engineering, Chung Yuan Christian University in Taiwan, from 2011 to 2014, an Associate Professor with the Department of Electronic Engineering, Chung Yuan Christian University in Taiwan, from 2014 to 2017, where he has been a Professor with the Department of Electronic Engineering, since 2017. His current research interests include VLSI chip design, image processing, wireless body sensor network, internet of things, wearable devices, data compression, fuzzy logic control, bio-medical signal processing, and reconFigureurable architecture.

Dr. Chen was a recipient of the Outstanding Teaching Award from Chung Yuan Christian University in 2014 and 2019, respectively.

Yu-Chieh Chu received her B.S. and M.S. degrees from the Department of Electrical and Computer Engineering, Tamkang University (TKU), Taiwan, in 2015 and 2017, respectively, and Ph.D. degree from the Department of Mechanical and Intelligent Systems Engineering at the University of Electro-Communications (UEC), Tokyo, Japan in 2021. She is currently an Assistant Professor in the Department of Electrical Engineering at Chung Yuan Christian University (CYCU), Taoyuan City, Taiwan. Her research interests include robotics, intelligent systems, machine learning and nonlinear systems control.

Xin-Yu Chen is currently studying Electronic Engineering and Computer Science at Chung Yuan Christian University, Zhongli, Taoyuan, Taiwan in 2023. Her current research interests include VLSI chip design, image processing and machine learning.

Pei-Chen Wu is currently studying Electronic Engineering and Computer Science at Chung Yuan Christian University, Zhongli, Taoyuan, Taiwan in 2023. Her current research interests include VLSI chip design, image processing and machine learning.

Patricia Angela Abu is the research lab head of the Ateneo Laboratory for Intelligent Visual Environment (ALIVE) and is an Assistant Professor at the Department of Information Systems and Computer Science (DISCS) at the Ateneo de Manila University. Her current research focuses on image processing and computer vision with applications that revolve on biomedical imaging and road/transportation, anomaly detection and IoT systems which granted ALIVE several best research paper and presentation awards both local and abroad. Dr. Abu received her M.S. degree in Electronics Engineering Major in Microelectronics from Chung Yuan Christian University, Chung-Li, Taiwan in 2009. She received both her Ph.D. in Computer Science and B.S. in Electronics and Communications Engineering degrees from the Ateneo de Manila University, Philippines in 2007 and 2012, respectively.